

Improving Action Smoothness for a Cascaded Online Learning Flight Control System

Yifei Li¹ and Erik-Jan van Kampen²

Abstract—This paper aims to improve the action smoothness of a cascaded online learning flight control system. Although the cascaded structure is widely used in flight control design, its stability can be compromised by oscillatory control actions, which poses challenges for practical engineering applications. To address this issue, we introduce an online temporal smoothness technique and a low-pass filter to reduce the amplitude and frequency of the control actions. Fast Fourier Transform (FFT) is used to analyze policy performance in the frequency domain. Simulation results demonstrate the improvements achieved by the two proposed techniques.

Index Terms—reinforcement learning, symmetry, data augmentation, approximate policy iteration, flight control.

I. INTRODUCTION

In the past decades, model-based control (MBC) design has played a major role in the field of flight control. With a well-calibrated model of real-world flight dynamics, including aerodynamic coefficients, actuator dynamics, the dynamic characteristics of aerial flight can be effectively represented and analyzed [1]. The modeling of aerodynamics offers benefits for flight control design in terms of interpretability, directionality, and effectiveness. Specifically, MBC design seeks to formulate the control law as the inverse of a model, thereby canceling the system dynamics. Representative examples include nonlinear dynamic inversion (NDI) [2], [3], [4], backstepping (BS) [5], and sliding mode control (SMC) [6]. However, these MBC methods are limited by model uncertainties, which increase the computational cost of model inversion and degrade control performance. To address this issue, uncertainty and disturbance estimation and attenuation techniques have been commonly employed alongside MBC. These methods estimate unmodeled dynamics and external disturbances by leveraging measured data, while simultaneously compensating through the control law [7]. Common examples include the disturbance observer (DOB) and extended state observer (ESO). Nevertheless, observer design also depends on a system model to compute estimation errors.

In contrast, data-driven control techniques leverage system data to design and refine control laws, opening a broad design space for model-free control (MFC), which seeks to reduce reliance on system models. Although hybrid control

approaches that integrate both system models and samples have improved the adaptability of model-based control, their capacity to optimize control performance is still a challenge. Examples of these methods are adaptive NDI [8], [9], [10], [11] and adaptive backstepping [12], [13], [14]. A fully model-free control design is exemplified by model-free reinforcement learning (RL), a learning-based approach that minimizes reliance on system models [15]. In this framework, the control law can be parameterized as an Artificial Neural Network (ANN) and trained using system samples. The training process is viewed as policy optimization, guided by a critic network that approximates the value function. Another key component of the RL framework is policy evaluation, where the critic network is trained based on the principle of Temporal-Difference (TD) learning. In model-based reinforcement learning, a system model is still used to make one- or multi-step state predictions. However, model inaccuracies have been shown to cause only limited degradation in control performance [16].

The online implementation of RL, referred to here as *on-line learning*, focuses on learning from state and cost signals measured directly from a real system that cannot be reset. This implementation involves multiple updates to the critic and actor networks before executing an action on the physical system. Such an approach enables adaptive adjustment of the control law via gradient-based optimization, thereby expanding the applicability of RL to adaptive flight control, which deals with unpredictable model uncertainties. This has been investigated for both fixed-wing and rotor-wing unmanned aerial vehicles using a class of incremental model-based approximate dynamic programming methods that support online system identification and policy learning [16], [17], [18], [19], [20], [21], [22], [23]. A representative example is Incremental Heuristic Dynamic Programming (IHDP) [19], [24], [25], which employs an incremental model to linearly approximate the nonlinear system. This approach reduces both the model complexity and the computational burden of online learning. Notably, the incremental model does not need to be highly accurate; it is sufficient for the signs of the estimated values to be correct in order to support effective policy optimization [24], [25].

Decomposing the dynamical system into reduced-order subsystems before control design can simplify the learning process in learning-based control frameworks. For instance, the pitch-rate dynamics is modeled as a first-order mapping from control surface deflection to pitch rate (see Equation 1). In this case, the value function associated with pitch rate tracking error and control effort is directly related

¹Yifei Li is with the Faculty of Aerospace Engineering, Delft University of Technology, 2629HS, Delft, The Netherlands Y.Li-34@tudelft.nl

²Erik-Jan van Kampen is with the Faculty of Aerospace Engineering, Delft University of Technology, Delft, 2629HS, The Netherlands E.vanKampen@tudelft.nl

to the actor network [26]. However, this design approach cannot be directly extended to angle-of-attack tracking, as the value function associated with tracking error fails to provide effective gradients for training control surface actor due to its indirect control effect on the angle of attack [1]. This requires a well-trained critic to provide accurate gradients, which is challenging in online learning due to limited sample availability. To address this, a *hierarchical* control strategy can be employed, separating the angle-of-attack and pitch-rate dynamics into two subsystems for independent control design [12], [13], [14], [27]. A virtual pitch-rate command is first designed to control the angle of attack. This virtual command then serves as the reference for the pitch-rate tracking control system, resulting in a cascaded control structure. This design is reflected in many flight control applications [24], [28]. The cascaded structure not only facilitates the integration of pitch-rate constraints but also simplifies the learning process by preventing the RL agent from using aggressive actions in the absence of such constraints. A practical example of this approach is the control of the F-16 Fighting Falcon using incremental global dynamic heuristic programming [20].

One key concern in upgrading cascaded online learning flight control systems is ensuring the smoothness of both virtual and actual control actions. Action smoothness significantly affects tracking performance and system stability [20], [22]. A common strategy to promote smooth action transitions is the use of an action smoothness loss for actor training. The design of this loss depends on how action variation is defined, such as temporal or spatial variations [29]. While these methods have shown effectiveness in offline-trained control systems for quadrotors [29], they have not yet been applied in online learning scenarios. In addition, introducing a low-pass filter between sub-control systems can help suppress high-frequency signals of the virtual control actions, thereby enhancing action smoothness. This approach has been successfully implemented in command-filtered INDI and backstepping [5], [30], [31]. However, the integration of a filter into a cascaded online learning flight control framework remains unexplored.

The main contributions of this paper are summarized as

- An optimization-based cascaded flight control system is developed to achieve angle-of-attack tracking.
- A *hybrid* approach combining online temporal smoothness and a low-pass filter is developed to improve actions smoothness of the cascaded online learning flight control system.
- A thorough analysis of the online learning control performance is conducted from multiple perspectives, such as the actor sensitivity, the saturation level of activation function.

The remainder of this paper is structured as follows. Section II presents the aerial vehicle dynamics and a discrete-time model. Section III presents optimization-based control design for angle-of-attack tracking. Section IV presents the online learning framework, followed by the introductions of

two action smoothness techniques in Section V. Section VI presents comparative simulations of control systems with action smoothness techniques. Section VII concludes this paper.

II. MODEL

This section introduces the longitudinal dynamical model of aerial vehicles. The discrete-time model is then derived based on the Euler method for convenient flight control design.

A. Dynamics

The nonlinear dynamical equations of aerial vehicles are given as [32]

$$\begin{aligned}\dot{\alpha} &= \left(\frac{fgQS}{WV}\right) \cos(\alpha)[\phi_z(\alpha) + b_z\delta] + q \\ \dot{q} &= \left(\frac{fQScd}{I_{yy}}\right)[\phi_m(\alpha) + b_m\delta]\end{aligned}\quad (1)$$

where α, q are angle-of-attack, pitch rate, δ is the control surface deflection. The aerodynamic coefficients are approximately computed by $b_z = -0.034, b_m = -0.206$, and

$$\begin{aligned}\phi_z(\alpha) &= 0.000103\alpha^3 - 0.00945\alpha|\alpha| - 0.170\alpha \\ \phi_m(\alpha) &= 0.000215\alpha^3 - 0.0195\alpha|\alpha| - 0.051\alpha\end{aligned}\quad (2)$$

These approximations of $b_z, b_m, \phi_z(\alpha), \phi_m(\alpha)$ hold for α in the range of ± 20 degrees. The physical coefficients are provided in Table I. In addition, the actuator dynamics are considered as a first order model with the time constant $0.005s$. The rate limit is 600 deg/s , and a control surface deflection limit is ± 20 degrees.

TABLE I
PHYSICAL PARAMETERS (ADAPTED FROM [32])

Notations	Definition	Value
g	acceleration of gravity	9.815 m/s ²
W	weight	204.3 kg
V	speed	947.715 m/s
I_{yy}	pitch moment of inertia	247.438 kg·m ²
f	radians to degrees	180/π
Q	dynamic pressure	29969.861 kg/m ²
S	reference area	0.041 m ²
d	reference diameter	0.229 m

B. Discretization

The state derivative can be approximated using the Euler method as

$$\begin{aligned}\dot{\alpha}_t &\approx \frac{\alpha_{t+1} - \alpha_t}{T} \\ \dot{q}_t &\approx \frac{q_{t+1} - q_t}{T}\end{aligned}\quad (3)$$

where t is the index of discrete time steps, T is the time step size.

Therefore, Equations 1 are approximately written as

$$\begin{aligned}\frac{\alpha_{t+1} - \alpha_t}{T} &= f_1(\alpha_t) + d(\alpha_t, \delta_t) + q_t \\ \frac{q_{t+1} - q_t}{T} &= f_2(\alpha_t) + g\delta_t\end{aligned}\quad (4)$$

where

$$\begin{aligned}f_1(x_1) &= \left(\frac{fgQS}{WV}\right) \cos(x_1)\phi_z(x_1) \\ d(x_1, u) &= \left(\frac{fgQS}{WV}\right) \cos(x_1)b_z u \\ f_2(x_1) &= \left(\frac{fgQS}{WV}\right) \phi_m(x_1) \\ g &= \left(\frac{fgQS}{WV}\right) b_m\end{aligned}\quad (5)$$

Rewrite Equation 6 as:

$$\begin{aligned}\alpha_{t+1} &= h_1(\alpha_t, q_t, \delta_t) \\ q_{t+1} &= h_2(q_t, \alpha_t, \delta_t)\end{aligned}\quad (6)$$

where

$$\begin{aligned}h_1(\alpha_t, \delta_t, q_t) &= \alpha_t + T(f_1(\alpha_t) + d(\alpha_t, \delta_t) + q_t) \\ h_2(\alpha_t, \delta_t, q_t) &= q_t + T(f_2(\alpha_t) + g\delta_t)\end{aligned}\quad (7)$$

III. OPTIMIZATION-BASED CONTROL DESIGN

Define the tracking errors as $e_{\alpha(t)} = \alpha_t - \alpha_{\text{ref}(t)}$, $e_q = q_t - q_{\text{ref}(t)}$. The $e_{\alpha(t+1)}$ is computed as

$$\begin{aligned}e_{\alpha(t+1)} &= \alpha_{t+1} - \alpha_{\text{ref}(t+1)} \\ &= \alpha_t + T(f_1(\alpha_t) + d(\alpha_t, \delta_t) + q_t) - \alpha_{\text{ref}(t+1)} \\ &= \alpha_t + T(f_1(\alpha_t) + d(\alpha_t, \delta_t) + q_t - q_{\text{ref}(t)} + q_{\text{ref}(t)}) \\ &\quad - \alpha_{\text{ref}(t+1)} \\ &= \alpha_t + T(f_1(\alpha_t) + d(\alpha_t, \delta_t) + e_{\alpha(t)} + q_{\text{ref}(t)}) \\ &\quad - \alpha_{\text{ref}(t+1)}\end{aligned}\quad (8)$$

Define a virtual control $q_{\text{ref}(t)} = v(e_{\alpha(t)}, \alpha_t)$, which is associated with e_{α}, α to provide error-feedback control for stabilizing $e_{\alpha(t)}$ and compensate for the system dynamics associated with α_t . However, when the system dynamics are unknown, an analytical design of the virtual control law $v(e_{\alpha(t)}, \alpha_t)$ is infeasible. In such cases, $v(e_{\alpha(t)}, \alpha_t)$ can be parameterized by a neural network as $v(e_{\alpha(t)}, \alpha_t) = W^{\vartheta_1}(e_{\alpha(t)}, \alpha_t)$ and optimized with samples. ϑ_1 denotes the parameter set of neural network.

The value function is defined as a quadratic function of the tracking error and the virtual control:

$$V_1(t) = \sum_{i=t}^{\infty} (e_{\alpha(i+1)}^2 + a v^2(e_{\alpha(i)}, \alpha_i)) \quad (9)$$

where $a > 0$ is a weighting parameter that balances the trade-off between the quadratic state term and the quadratic control term.

Then the virtual control law is defined as

$$v^*(e_{\alpha(t)}, \alpha_t, \delta_t) = \arg \min_{v_t} V_1(t) \quad (10)$$

The $e_{q(t+1)}$ is computed as

$$\begin{aligned}e_{q(t+1)} &= q_{t+1} - q_{\text{ref}(t+1)} \\ &= q_t + T(f_2(\alpha_t) + g\delta_t) - q_{\text{ref}(t+1)}\end{aligned}\quad (11)$$

The control surface deflection $\delta_t = u(e_{q(t)}, q_t)$ is designed as a function of $e_{q(t)}$ and q_t to provide error-feedback for stabilizing $e_{q(t)}$ and compensate for the system dynamics associated with q_t . However, since the system dynamics $f_2(\cdot), g$ and $q_{\text{ref}(t+1)}$ are unknown, the control law $u(e_{q(t)}, q_t)$ cannot be explicitly designed. Instead, $u(e_{q(t)}, q_t)$ is parameterized by a network as $u(e_{q(t)}, q_t) = W^{\vartheta_2}(e_{q(t)}, q_t)$, where ϑ_2 denotes the parameter set.

The value function is defined as:

$$V_2(t) = \sum_{i=t}^{\infty} (e_{q(i+1)}^2 + b u^2(e_{q(i)}, q_i, \alpha_i)) \quad (12)$$

where $b > 0$ is a weighting parameter.

The control law is designed as

$$u^*(e_{q(t)}, q_t, \alpha_t) = \arg \min_{u_t} V_2(t) \quad (13)$$

IV. ONLINE LEARNING IMPLEMENTATION

This section introduces a cascaded online learning framework in order to implement the optimization-based control design presented in Section III. This framework has been developed in References [20], [22], but its performance suffers from insufficient action smoothness. To improve action smoothness, we introduce a hybrid approach that combines online temporal smoothness technique and a low-pass filter.

A. Incremental heuristic dynamic programming

Incremental Heuristic Dynamic Programming (IHDP) is employed in the cascaded online learning framework to enable online policy learning [24]. This algorithm computes sub-optimal actions at states x_t , ($t = 0, 1, 2, \dots$), using an incremental model to generate one-step state transitions.

The incremental model for systems 6 is derived using Taylor expansion, expressed as

$$\begin{aligned}\Delta \hat{\alpha}_{t+1} &= F_{t-1}^1 \Delta \alpha_t + G_{t-1}^1 \Delta q_t \\ \Delta \hat{q}_{t+1} &= F_{t-1}^2 \Delta q_t + G_{t-1}^2 \Delta \delta_t\end{aligned}\quad (14)$$

The derivation is seen in Appendix A.

B. Cascaded control structure

The cascaded control system contains two separate RL agents, referred to as the higher-level agent and the lower-level agent, responsible for angle-of-attack and pitch rate tracking tasks, respectively. The higher-level agent learns a virtual control $v^*(e_{\alpha(t)}, \alpha_t, \delta_t)$ that minimizes the value function $V_1(t)$, while the lower-level agent learns a control $\delta^*(e_{q(t)}, q_t, \alpha_t)$ that minimizes $V_2(t)$. Both the critic and actor networks are initialized randomly, without incorporating any prior knowledge of the system dynamics. The design of a cascaded flight control framework is inspired by the backstepping method [12], [13], [14], [27]. The overall structure of the cascaded online learning control framework is illustrated in Figure 1.

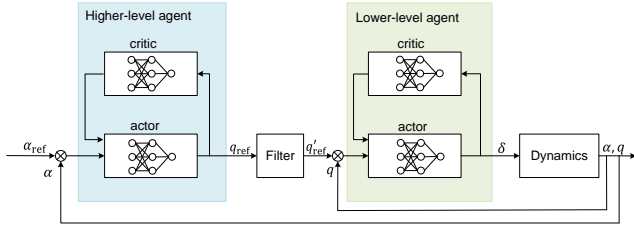


Fig. 1. Cascaded online learning flight control system. Two actors are connected in a cascaded structure to achieve angle-of-attack tracking using control surface deflection.

C. Higher-level agent

The higher-level agent aims to learn a virtual pitch rate reference for optimal angle-of-attack tracking, as defined in Equation 10. As is shown in Figure 2, the network topology is a single-hidden-layer perception. The critic network takes as input α_t and the tracking error $e_{\alpha(t)}$. Its output is the estimated value function $\hat{V}_1(t)$, with an absolute value activation function $\text{abs}(\cdot)$ applied at the output layer to ensure positive definiteness. The actor network use an additional input δ_t to account for the non-minimum phase dynamics in the α -dynamics, as shown in Equations 1. It outputs the virtual pitch rate command $q_{\text{ref}}(t)$, constrained by a scaled $\tanh(\cdot)$ activation function to satisfy action constraints. The target critic and actor networks share the same structures as the critic and actor.

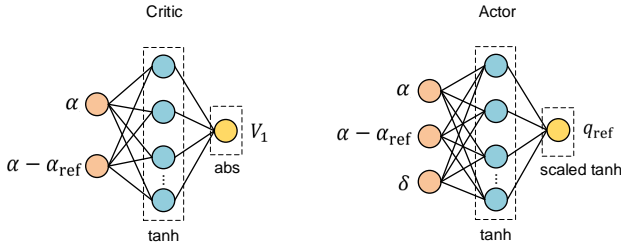


Fig. 2. The networks of the higher-level agent.

1) *Critic*: The critic network is updated through TD learning to minimize the quadratic TD error:

$$L_t^{C1} = \frac{1}{2} \delta_{1(t)}^T \delta_{1(t)} \quad (15)$$

$$\delta_{1(t)} = c_1(\hat{e}_{\alpha(t+1)}, q_t) + \gamma \hat{V}_{1\text{target}}(\hat{\alpha}_{t+1}, \hat{e}_{\alpha(t+1)}) - \hat{V}_1(\alpha_t, e_{\alpha(t)}) \quad (16)$$

$$c_1(\hat{e}_{\alpha(t+1)}, q_t) = \hat{e}_{\alpha(t+1)}^2 + a q_t^2 \quad (17)$$

2) *Actor*: The actor is updated to minimize the estimated state-value function:

$$v^*(\alpha_t, e_{\alpha(t)}, \delta_t) = \arg \min_{v_t} L_t^{A1} \quad (18)$$

$$L_t^{A1} = c_1(\hat{e}_{\alpha(t+1)}, q_t) + \gamma \hat{V}_{1\text{target}}(\hat{\alpha}_{t+1}, \hat{e}_{\alpha(t+1)})$$

The gradient-descent-based updates of critic and actor are seen in Appendix B.

D. Lower-level agent

The lower-level agent aims to learn the control surface deflection command for tracking the pitch rate reference. As shown in Equations 1, the control action δ introduces a non-minimal phase effect. As a result, the control surface may unintentionally influence α dynamics through the non-minimum phase effect. This is one of the key motivations for adopting a cascaded control structure, which isolates the non-minimum phase effect from the training process of the lower-level agent. In this way, the agent is prevented from attempting to control α through the non-minimum phase dynamics.

Figure 3 shows the network structures. The critic network takes as input the pitch rate q_t and the tracking error $e_{q(t)}$. The output is the estimated value function $V_2(t)$, with an absolute value activation applied at the output layer to ensure the positive definiteness of $V_2(t)$. The actor network utilizes an additional input α_t to account for dynamic coupling in model 1. The output is the control surface deflection δ_t . A scaled $\tanh(\cdot)$ activation function is applied to constrain the action within actuator limits. The target critic and actor networks share the same architectures as the critic and actor.

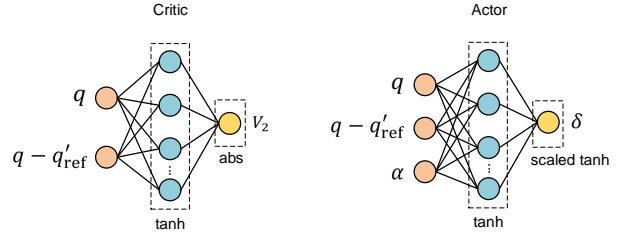


Fig. 3. The networks of the lower-level agent.

1) *Critic*: The critic is updated through TD learning to minimize a quadratic TD error, as

$$L_t^{C2} = \frac{1}{2} \delta_{2(t)}^T \delta_{2(t)} \quad (19)$$

$$\delta_{2(t)} = c_2(\hat{e}_{q(t+1)}, \delta_t) + \gamma \hat{V}_{2\text{target}}(\hat{q}_{t+1}, \hat{e}_{q(t+1)}) - \hat{V}(q_t, e_{q(t)}) \quad (20)$$

$$c_2(\hat{e}_{q(t+1)}, \delta_t) = \hat{e}_{q(t+1)}^2 + b \delta_t^2 \quad (21)$$

2) *Actor*: The actor is trained to minimize the estimated state-value function:

$$\delta^*(q_t, e_{q(t)}, \alpha_t) = \arg \min_{\delta_t} L_t^{A2} \quad (22)$$

$$L_t^{A2} = c_2(\hat{e}_{q(t)}, \delta_t) + \gamma \hat{V}_{2\text{target}}(\hat{q}_{t+1}, \hat{e}_{q(t+1)})$$

The gradient-descent-based updates of critic and actor are seen in Appendix C.

V. ACTION SMOOTHNESS TECHNIQUES

This section introduces a hybrid action smoothness approach that combines online temporal smoothness technique and low-pass filter, enabling actions smoothed in both time and frequency domains.

A. Online temporal action smoothness

In online learning, the actor is expected to be trained with less computation cost. To this end, only one sample is used for computing temporal smoothness loss online:

$$\begin{aligned} L_{\alpha(t)}^{\text{online}} &= |v(\hat{e}_{\alpha(t+1)}, \hat{\alpha}_{t+1}) - v(e_{\alpha(t)}, \alpha_t)| \\ L_{q(t)}^{\text{online}} &= |\delta(\hat{e}_{q(t+1)}, \hat{q}_{t+1}) - \delta(e_{q(t)}, q_t)| \end{aligned} \quad (23)$$

where \hat{x}_{t+1} is one-step prediction of state by a system model. In the case of IHDP, the incremental model is used to generate \hat{x}_{t+1} . Therefore, L_t^{online} can be efficiently computed in online learning with only a single forward propagation of model and actor.

Then the online temporal smoothness losses can be integrated into policy optimization through Lagrangian method:

$$\begin{aligned} v^*(e_{\alpha(t)}, \alpha_t, \delta_t) &= \arg \min_{v_t} \left(c_1(\hat{e}_{\alpha(t+1)}, q_t) \right. \\ &\quad \left. + \gamma \hat{V}_{1\text{target}}(\hat{e}_{\alpha(t+1)}, \hat{\alpha}_{t+1}) + \lambda_1 L_{\alpha(t)}^{\text{online}} \right) \\ \delta^*(e_{q(t)}, q_t, \alpha_t) &= \arg \min_{\delta_t} \left(c_2(\hat{e}_{q(t+1)}, \delta_t) \right. \\ &\quad \left. + \gamma \hat{V}_{2\text{target}}(\hat{e}_{q(t+1)}, \hat{q}_{t+1}) + \lambda_2 L_{q(t)}^{\text{online}} \right) \end{aligned} \quad (24)$$

where λ_1, λ_2 are the weights of loss terms $L_{\alpha(t)}^{\text{online}}, L_{q(t)}^{\text{online}}$. *Remark 1.* The temporal smoothness loss can be efficiently computed within a model-based online learning framework. The model can be used to predict one-step state transitions, which serve as the bias in a temporal smoothness loss.

Remark 2. Compared to the batch temporal smoothness loss in Reference [29], the online temporal smoothness loss uses a single sample so that the computation cost is reduced..

B. Low-pass filter

A low-pass filter is used to smoothen the pitch rate reference q_{ref} , which is formulated as a second-order dynamics as [30]

$$\begin{aligned} \dot{d}_1 &= d_2 \\ \dot{d}_2 &= -2\zeta\omega_n^2 d_2 - \omega_n^2(d_1 - q_{\text{ref}}) \end{aligned} \quad (25)$$

where d_1, d_2 are filtered signal and its differentiation, ω_n is the natural frequency, ζ is the damping factor.

VI. SIMULATION

This section provides simulation results of cascaded online learning flight control system using action smoothness techniques. The numerical simulation of aerial vehicle dynamics 1 are through fourth-order Runge Kutta method. The actuator dynamics is $\tau \dot{\delta}_t + \delta_t = \delta_{c(t)}, \tau = 0.005$. To constrain

actions, the actor networks to generate q_{ref} and δ are scaled to $20^\circ/s$. The angle-of-attack reference is set as $\alpha_{\text{ref}(t)} = 10^\circ \sin(\frac{2\pi}{T}t), T = 10s$. The hyperparameters used for the RL agents are listed in Table II. We consider the performance of control systems in aspects of action smoothness, saturation level of activation function, actor sensitivity and one-step costs.

TABLE II
HYPERPARAMETERS OF RL AGENTS

Parameter	Higher-level Agent	Lower-level Agent
critic learning rate η_{C_1}, η_{C_2}	0.1	0.1
actor learning rate η_{A_1}, η_{A_2}	5×10^{-7}	10^{-7}
discount factor γ	0.6	0.6
delay factor τ	1	1
policy iteration number at each time step	3	3
hidden layer size	7	7
critic hidden-layer activation function	tanh	tanh
critic output layer activation function	abs	abs
actor activation function	tanh	tanh
optimizer	Adam	Adam
control weight a, b	5×10^{-6}	10^{-5}
weight of temporal smoothness loss λ_1, λ_2	9.3×10^{-4}	10^{-5}
loss thresholds for terminating critic training	2.5×10^{-4}	5×10^{-5}
maximal number of critic and actor updates	50	50

A. Online temporal smoothness

1) *State and action:* Figure 4 shows that both the vanilla and TS-integrated flight control systems successfully track the reference signal $\alpha_{\text{ref}(t)}$. However, the vanilla control system owns sever state and action oscillations which degrade tracking error convergence, and finally diverges. In contrast, the TS-integrated control system promoting smoother control behavior and improves convergence of the system states, by penalizing the temporal variations of actions generated from actor networks.

Figure 5 shows that the parameters of critics converge to sub-optimum within 10s. However, the critic parameters of the vanilla control system continue to oscillate in response to tracking error fluctuations. In addition, for the higher-level agent, the parameters of the actor in the vanilla control system grows faster than those in the TS-integrated control system, due to larger oscillations of the tracking error e_{α} . The growth of parameters is slight for the lower-level agent's actors.

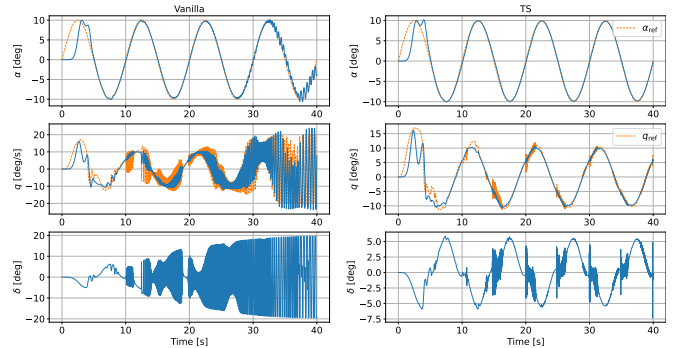


Fig. 4. Comparison between control systems without and with temporal smoothness loss.

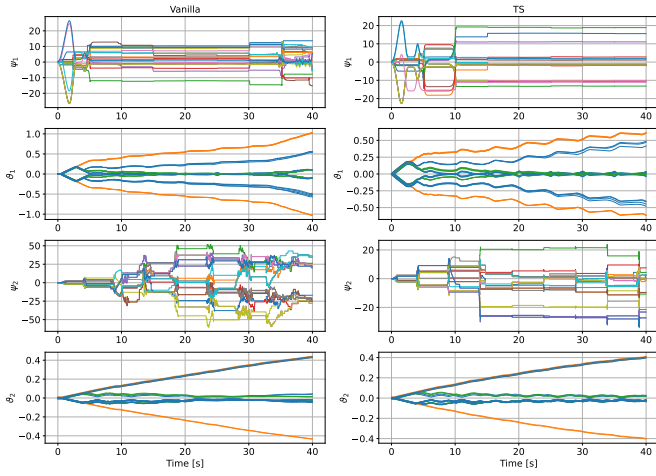


Fig. 5. Comparison of network parameters for flight control systems without and with using a temporal smoothness loss.

Figures 6 and Figure 7 provide detailed comparisons of the virtual control $q_{\text{ref}}(t)$ and control δ_t , respectively. The frequency-domain characteristics are visualized using the Fast Fourier Transform (FFT), which converts action series in the time domain into a frequency-domain representation. Figure 6 shows signals of $q_{\text{ref}}(t)$ within 100 Hz are effectively filtered with online TS technique¹. The amplitude of q_{ref} is reduced significantly without losing tracking performance. Similar results are seen for control surface deflection δ_t in Figure 7. A noteworthy reason for the oscillation of δ_t lies in that the switching $q_{\text{ref}}(t)$ causes switching tracking error $e_q(t)$ which is the input of the lower-agent's actor.

In the author's opinion, the TS loss can be understood as a prior information about the behavior of the expected controller, that uses flat actions to interact with the system. Therefore, by incorporating a TS loss, the RL agent is discouraged from producing aggressive control actions. Such actions may lead to saturation of the actor network's activation functions. This may further lead to vanishing of the gradient, making it difficult to go back to the gradient-sensitive zone. This indicates that the agent does not easily 'unlearn' a low-gain control policy once it learns a high-gain control policy. Consequently, the controller becomes inflexible to adjust to tracking errors and finally leads to divergence. This process is sufficiently exhibited in Figure 4.

2) *Action increment*: The one-step increment of virtual pitch rate reference is defined as

$$\Delta q_{\text{ref}}(t+1) = |q_{\text{ref}}(t+1) - q_{\text{ref}}(t)| \quad (26)$$

where $q_{\text{ref}}(t), q_{\text{ref}}(t+1)$ are actor outputs in $t+1, t$ and are defined as

$$q_{\text{ref}}(t+1) = W^{\vartheta_1}(\hat{e}_{\alpha}(t+1), \hat{\alpha}_{t+1}, \hat{\delta}_{t+1}) \quad (27)$$

¹The magnitude spectra in Figures 6, 7, 13, 14 are by the `numpy.fft.fft` function from Numpy library.

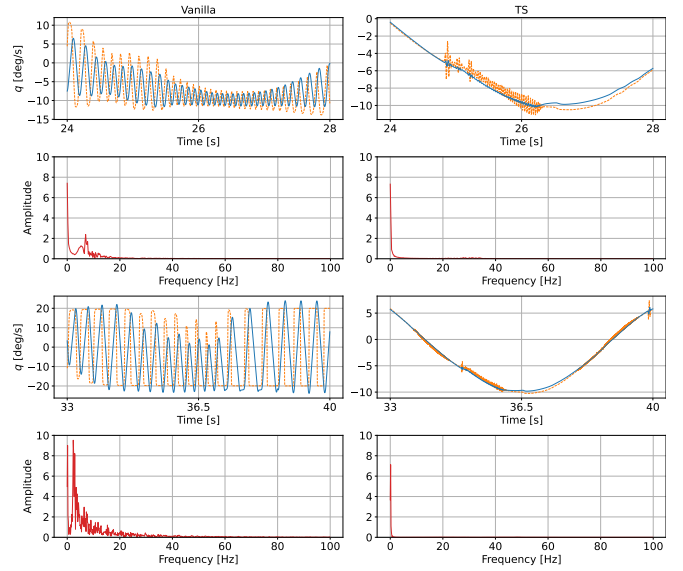


Fig. 6. Comparison of pitch rate reference in the time and frequency domains: without and with a TS loss.

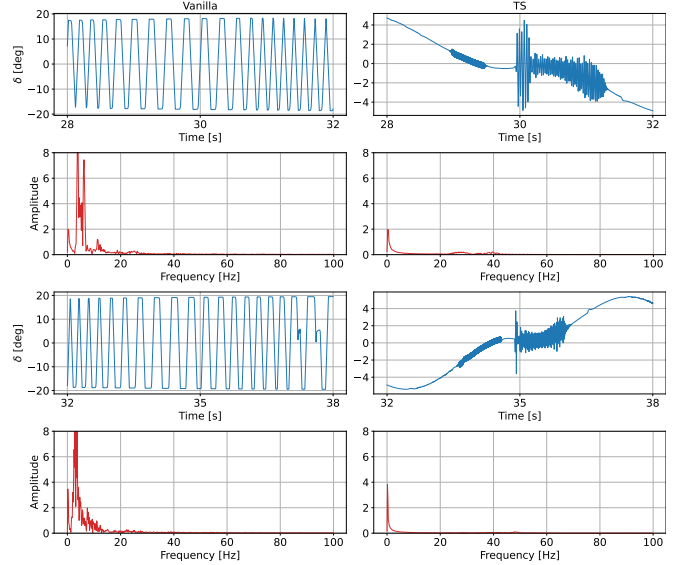


Fig. 7. Comparison of control surface deflection in the time and frequency domains: without and with a TS loss.

$$q_{\text{ref}}(t) = W^{\vartheta_1}(e_{\alpha}(t), \alpha_t, \delta_t) \quad (28)$$

The one-step increment of control surface deflection is

$$\Delta \delta_{t+1} = |\delta_{t+1} - \delta_t| \quad (29)$$

where δ_{t+1}, δ_t are actor network outputs in $t+1, t$ and are defined as:

$$\begin{aligned} \delta_{t+1} &= W^{\vartheta_2}(\hat{e}_q(t+1), \hat{q}_{t+1}, \hat{\alpha}_{t+1}) \\ \delta_t &= W^{\vartheta_2}(e_q(t), q_t, \alpha_t) \end{aligned} \quad (30)$$

Figure 8 compares the histories of action increments. The TS loss for the higher-level agent reduces the amplitude of $|\Delta q_{\text{ref}}(t+1)|$ to less than 0.5 deg/s. For lower-level agent, the

reduction of the amplitude of $|\Delta\delta(t)|$ is restricted by control surface deflection limits. The reason lies in that the vanilla control system does not penalize aggressive actions so that it learns a 'bang-bang' control strategy to reduce tracking errors, while the TS loss penalizes fast changes of actions so that a low-gain control law is learned.

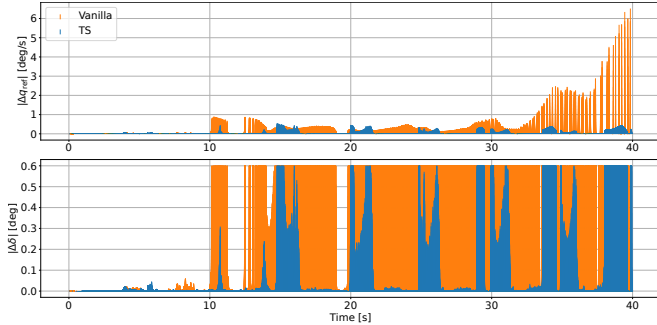


Fig. 8. Comparison of actors' output increments over time.

3) *One-step cost*: Figure 9 compares one-step costs over time during online learning. For the higher-level agent, TS method provides small one-step costs in a starting phase [0-10]s. The one-step cost of the vanilla control system shows oscillations in a final learning phase [30-40]s because of the failure of angle of attack tracking (see Figure 6). This failure is explained by a high-gain control law learned during continual learning. As a comparison, TS method avoids the agent learning a high-gain control law by constraining action increments over time.

For the lower-level agent, the oscillations of one-step costs in the vanilla control system are more obvious due to the unsuccessful tracking of pitch rate reference. The virtual control command q_{ref} is a high-frequency oscillatory signal that brings difficulty into tracking (see Figure 4).

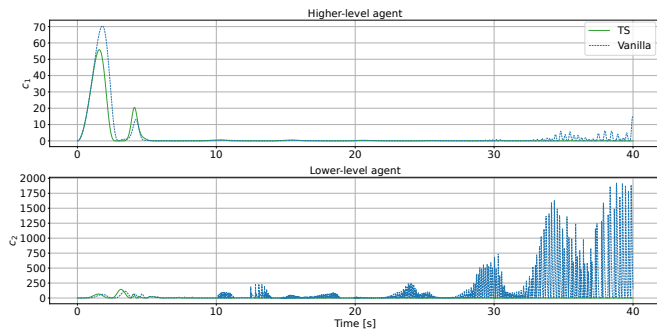


Fig. 9. Comparison of one-step costs without and with the TS loss. TS method enables lower one-step costs and a stable learning process free of significant fluctuations.

4) *Activation function saturation level*: The saturation of an activation function $\tanh(\cdot)$ indicates its output approaches the maximum or minimum value due to large amplitude of input (see Figure 10). Meantime, its gradient vanishes and finally approaches zero. The vanishing gradient leads to slow-pace learning of control policy through gradient descent approaches. A worse effect is that a saturated activation

function outputs maximum or minimum actions in response to tracking errors, resulting in a 'bang-bang' control effect. This 'bang-bang' control effect will degrade tracking control performance and system stability.

The 'bang-bang' control strategy is usually learned through an overly aggressive learning process. Specifically, the reasons can be: (1) the RL agent uses a large learning rate. A large learning rate causes the actor's weights to be updated with large increments, pushing the activation function into its saturation zone. (2) An inadequately tuned loss function. A loss function that underemphasizes the control effort can lead to comparable outcomes. In such cases, the actor learns to generate large control actions in response to tracking errors, without properly accounting for control effort. These large actions typically arise from saturated activation functions. Moreover, this aggressive learning behavior may persist even as the tracking error decreases, continuing to degrade control performance.

Figure 10 shows the dynamical saturation level of the activation function in output layer of actors. The vanilla control system eventually makes $\tanh(\cdot)$ saturated in the range of input intervals $[-4,-2]$, $[2,4]$ (the higher-level agent), and input intervals $[-3,-2]$, $[2,3]$ (the lower-level agent). In these intervals, the derivative of $\tanh(\cdot)$ is less than 0.1, providing slight gradient for actor training. As a comparison, the TS-integrated control system avoids the saturation even starting with the same setting as the vanilla control system. The input of $\tanh(\cdot)$ is kept within 'unsaturated' intervals $[-2,2]$ (the higher-level agent) and $[-0.5,0.5]$ (the lower-level agent). This demonstrates the effectiveness of a TS loss to avoid saturation of $\tanh(\cdot)$.

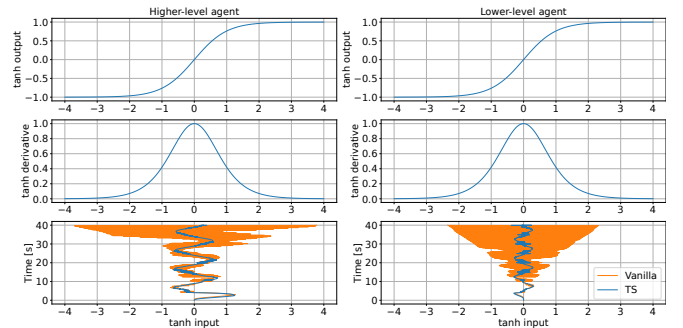


Fig. 10. Comparison of activation function $\tanh(\cdot)$ saturation level in the output layer of actors during the online learning phase: without and with a TS loss.

5) *Sensitivity analysis*: The sensitivity of the actor indicates how much the output will change, and in what direction, if the input slightly increases [34]. High sensitivity may cause the actor to overreact to states variations and overcorrect the tracking error. This is also correlated to robustness of the actor against sensor noise and uncertainties.

The sensitivity measures for actors are defined as

$$K_{1(t)} = \frac{\partial q_{ref}(t)}{\partial e_{\alpha}(t)} \quad (31)$$

$$K_{2(t)} = \frac{\partial \delta(t)}{\partial e_q(t)} \quad (32)$$

where $e_{\alpha(t)} = \alpha_t - \alpha_{\text{ref}(t)}$, $e_q(t) = q_t - q'_{\text{ref}(t)}$ are tracking errors, $K_{1(t)}$, $K_{2(t)}$ are sensitivity measures.

Figure 11 compares sensitivity measures. The vanilla control system shows oscillations of measures, indicating the actor is significantly sensitive to error variants. The TS-integrated control system shows reduced oscillations because the TS loss penalizes the increments of actions. The action increments are determined by actor sensitivity.

The relation between the virtual control and its sensitivity measure is

$$\begin{aligned} & |q_{\text{ref}(t+1)} - q_{\text{ref}(t)}| \\ & \approx |K_{1(t)}(e_{\alpha(t+1)} - e_{\alpha(t)})| \\ & = |K_{1(t)}| \cdot |e_{\alpha(t+1)} - e_{\alpha(t)}| \end{aligned} \quad (33)$$

Similarly, the relation between control surface deflection and its sensitivity measure is

$$\begin{aligned} & |\delta_{(t+1)} - \delta_{(t)}| \\ & \approx |K_{2(t)}(e_q(t+1) - e_q(t))| \\ & = |K_{2(t)}| \cdot |e_q(t+1) - e_q(t)| \end{aligned} \quad (34)$$

Equations 33, 34 show that the increments of (virtual) action can be reduced through reducing sensitivity. This is demonstrated in Figure 11.

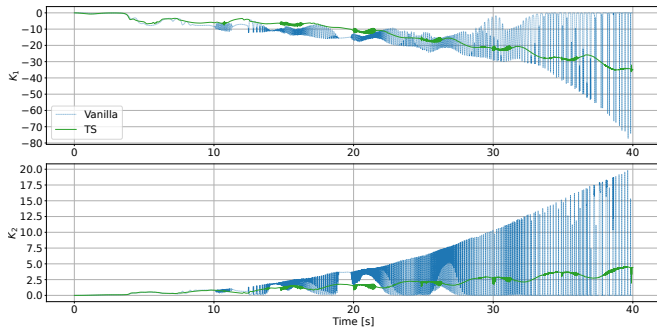


Fig. 11. Comparison of sensitivity measures before and after using a TS loss. Actor 1, 2 represent the actors of higher-level and lower-level agents.

6) *Challenges*: The online temporal smoothness technique helps the actor to produce smoother actions, but the weight tuning is empirical. An inappropriately large weight slows down the process of actor training, while an inappropriately small weight may show degraded smoothness effect. The selection of an appropriate weight for the temporal smoothness loss remains an unresolved issue.

On the other hand, Figure 12 shows that the TS loss does not eliminate small-amplitude, high-frequency oscillations, as its effect diminishes when the magnitude of action increments is small. In this situation, a low-pass filter shows its ability of filtering high-frequency commands in frequency domain perspective, and thus reduces low-amplitude, high-frequency oscillations. Meanwhile, incorporating a low-pass filter into the flight control system does not interfere with the training of the actor network.

B. Command filter

The command filter technique has been applied for cascaded model-based flight control systems to filter out the high-frequency signals of virtual pitch rate [5]. In this subsection, we use a low-pass filter in the cascaded online learning flight control system. The filter parameters are given in Table III.

TABLE III
FILTER PARAMETERS

Parameter	Value
Damping factor ζ	0.7
natural frequency ω_0	20 rad/s

Figure 12 compares angle-of-attack tracking performance. The first control system uses online temporal smoothness technique, the second control system uses both online temporal smoothness technique and a low-pass filter. It is shown that the filter is capable of migrating high-frequency oscillations of virtual pitch rate reference, and enables smooth control surface deflections. Figure 13 shows detailed comparisons on virtual pitch rate reference in short time periods. It is observed that the signals of q_{ref} in [10-40]Hz are effectively eliminated by the filter. Figure 14 provides detailed comparisons on δ in short time periods. It is observed that oscillations over [10-40]Hz are effectively migrated. This performance is achieved through a specific set of filter parameters.

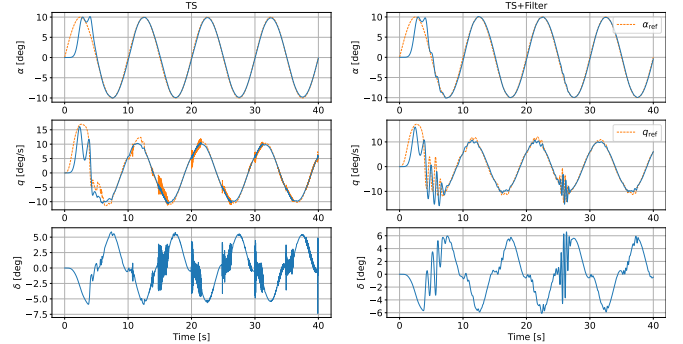


Fig. 12. Comparison of control performance: TS versus TS+Filter.

1) *One-step cost*: Figure 15 compares the one-step costs during the online learning phase. For the higher-level agent, the one-step costs of using the TS method and TS + Filter method are similar. This is primarily because the quadratic action term in the one-step cost function carries a small weight, and the TS method is sufficient to achieve angle-of-attack tracking. In contrast, for the lower-level agent, the TS + Filter method results in significantly lower one-step costs during the initial learning phase [0-15]s compared to the TS method. During the learning phase [10-30]s, the filter shows its ability to reduce cost oscillations. This is implemented by smoothing the reference q_{ref} which is fed to the lower-level agent to generate refined pitch rate tracking errors.

2) *Activation function saturation level*: Figure 16 shows the dynamical saturation level of the activation function

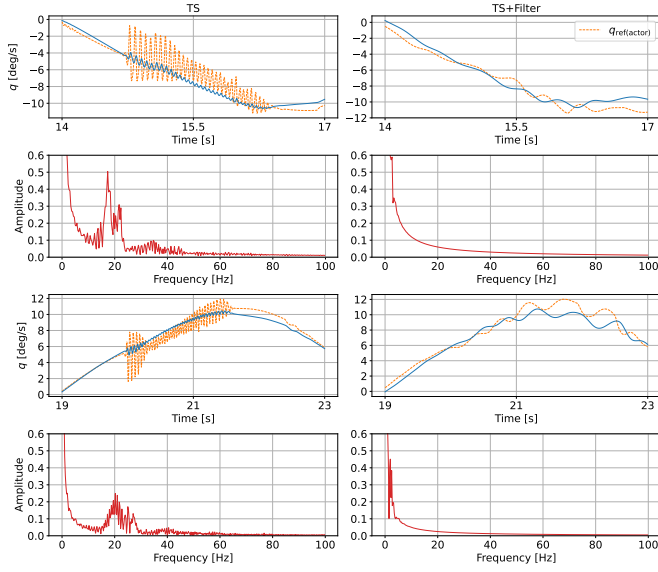


Fig. 13. Detailed comparison of pitch rate tracking in the time and frequency domains between TS method and TS+Filter method

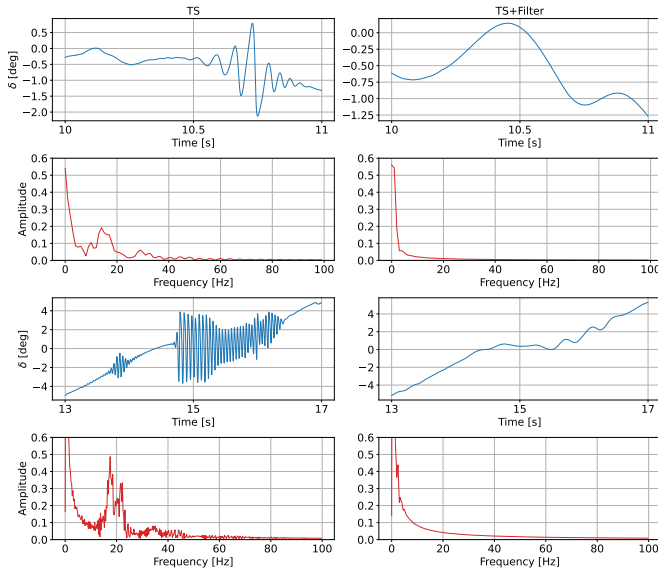


Fig. 14. Detailed comparison of control surface deflection in the time and frequency domains between TS and TS+Filter methods.

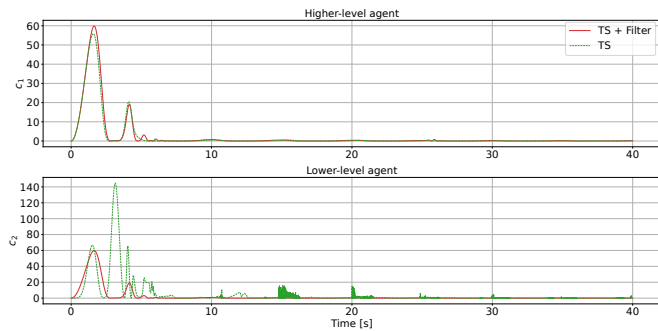


Fig. 15. Comparison of one-step cost of two control systems using the TS method and TS+Filter method.

$\tanh(\cdot)$ in the output layer of actors. Both the TS method and TS + Filter method effectively prevent saturation of $\tanh(\cdot)$, ensuring that its gradient remains within the sensitive, non-vanishing region and supporting effective learning.

3) *Sensitivity analysis*: Figure 17 compares the sensitivity measures $K_1(t)$ and $K_2(t)$. The results show that the use of a filter slows the growth of the measures and reduces their oscillations, contributing to a more robust controller.

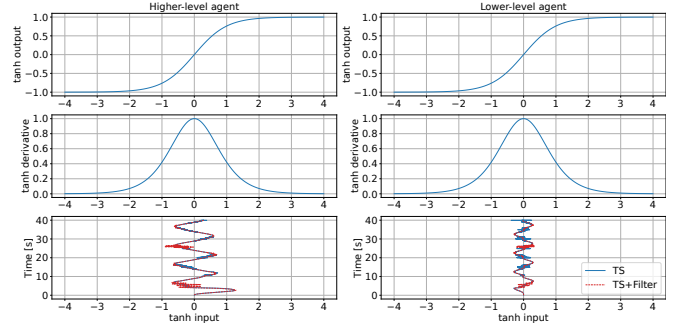


Fig. 16. Comparison of saturation level of activation function $\tanh(\cdot)$ in the output layer of actors during the online learning phase: without and with a low-pass filter.

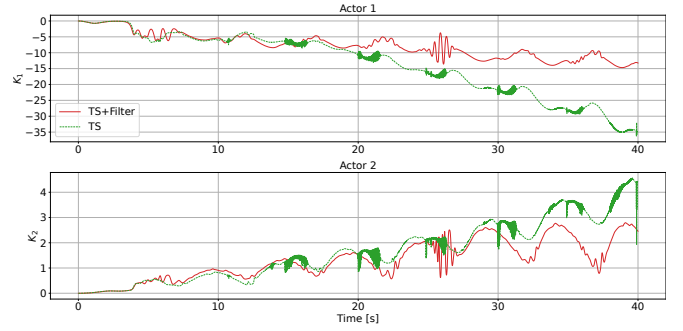


Fig. 17. Comparison of sensitivity measures between TS method and TS+Filter method.

VII. CONCLUSION

In this paper, a cascaded online learning flight control system is developed for angle-of-attack tracking. We introduced two techniques to improve action smoothness: online temporal smoothness and low-pass filter. Online temporal smoothness is verified through simulation to effectively reduce the amplitude of virtual pitch rate reference and control surface deflection. The low-pass filter is able to remove the high-frequency signals of pitch rate reference from a frequency domain, which can not be achieved by only using online temporal smoothness technique. Therefore, a *hybrid* approach that combines temporal smoothness and a low-pass filter makes the best benefit of improving action smoothness.

REFERENCES

- [1] J. D. Anderson *Fundamentals of Aerodynamics*. McGraw-Hill Series in Aeronautical and Aerospace Engineering. New York, USA: McGraw-Hill, 2017.

- [2] S. Sieberling, Q. P. Chu, and J. A. Mulder Robust Flight Control Using Incremental Nonlinear Dynamic Inversion and Angular Acceleration Prediction *Journal of Guidance, Control and Dynamics*, vol. 33, no. 6, pp. 1732–1742, 2010, doi: 10.2514/1.49978.
- [3] X. R. Wang, E. van Kampen, Q. P. Chu and P. Lu Stability Analysis for Incremental Nonlinear Dynamic Inversion Control *Journal of Guidance, Control and Dynamics*, vol. 42, no. 5, pp. 1116–1129, 2019, doi: 10.2514/1.G003791.
- [4] Z. C. Liu, Y. F. Zhang, and J. J. Liang and H. X. Chen Application of the Improved Incremental Nonlinear Dynamic Inversion in Fixed-Wing UAV Flight Tests *Journal of Aerospace Engineering*, vol. 35, no. 6, pp. 1–13, 2022, doi: 10.1061/(ASCE)AS.1943-5525.0001495.
- [5] Y. C. Wang, W. S. Chen, S. X. Zhang, J. W. Zhu and L. J. Cao Command-Filtered Incremental Backstepping Controller for Small Unmanned Aerial Vehicles *Journal of Guidance, Control, and Dynamics*, vol. 41, no. 4, pp. 952–965, 2018, doi: 10.2514/1.G003001.
- [6] X. R. Wang, E. van Kampen, Q. P. Chu and P. Lu Incremental Sliding-Mode Fault-Tolerant Flight Control *Journal of Guidance, Control, and Dynamics*, vol. 42, no. 2, pp. 244–259, 2019, doi: 10.2514/1.G003497.
- [7] W. H. Chen, J. Yang, L. Guo and S. H. Li Disturbance-Observer-Based Control and Related Methods—An Overview *IEEE Transactions on Industrial Electronics*, vol. 63, no. 2, pp. 1083–1095, 2016, doi: 10.1109/TIE.2015.2478397.
- [8] D. M. Acosta and S. S. Joshi Adaptive Nonlinear Dynamic Inversion Control of an Autonomous Airship for the Exploration of Titan *AIAA Guidance, Navigation and Control Conference and Exhibit*, Hilton Head, South Carolina, USA, August, 2007, doi: 10.2514/6.2007-6502.
- [9] E. J. J. Smeur, Q. P. Chu and G. H. E. de Croon Adaptive Incremental Nonlinear Dynamic Inversion for Attitude Control of Micro Air Vehicles *Journal of Guidance, Control, and Dynamics*, vol. 39, no. 3, pp. 450–461, 2016, doi: 10.2514/1.G001490.
- [10] B. Smit, T. S. C. Pollack and G. S. Tallen Adaptive Incremental Nonlinear Dynamic Inversion Flight Control for Consistent Handling Qualities *AIAA SciTech 2022 Forum*, San Diego, CA&Virtual, USA, January, 2022, doi: 10.2514/6.2022-1394.
- [11] J. Harris, C. M. Elliott and G. S. Tallen L1 Adaptive Nonlinear Dynamic Inversion Control for the Innovative Control Effectors Aircraft *AIAA SciTech 2022 Forum*, San Diego, CA&Virtual, USA, January, 2022, doi: 10.2514/6.2022-0791.
- [12] L. Sonneveldt, Q. P. Chu and J. A. Mulder Constrained Adaptive Backstepping Flight Control: Application to a Nonlinear F-16/MATV Model *AIAA Guidance, Navigation and Control Conference and Exhibit*, Keystone, Colorado, USA, August, 2006, doi: 10.2514/6.2006-6413.
- [13] L. Sonneveldt, Q. P. Chu and J. A. Mulder Nonlinear Flight Control Design Using Constrained Adaptive Backstepping *Journal of Guidance, Control, and Dynamics*, vol. 30, no. 2, pp. 322–336, 2007, doi: 10.2514/1.25834.
- [14] Q. Hu, Y. Meng, C. L. Wang and Y. M. Zhang Adaptive Backstepping Control for Air-breathing Hypersonic Vehicles with Input Nonlinearities *Aerospace Science and Technology*, vol. 73, pp. 289–299, 2018, doi: 10.1016/j.ast.2017.12.001.
- [15] R. S. Sutton and A. G. Barto *Reinforcement Learning: An Introduction*. 6th edition, Sigma Series in Pure Mathematics. Cambridge, MA, USA: A Bradford Book, 2018.
- [16] Y. Zhou, E. van Kampen and Q.P. Chu Incremental Model Based Online Dual Heuristic Programming for Nonlinear Adaptive Control *Control Engineering Practice*, vol. 73, pp. 13–25, 2018, doi: 10.1016/j.conengprac.2017.12.011.
- [17] Y. Zhou, E. van Kampen and Q. P. Chu Incremental Approximate Dynamic Programming for Nonlinear Flight Control Design In *Proceedings of the EuroGNC 2015*, Toulouse, France, 2015.
- [18] Y. Zhou, E. van Kampen and Q. P. Chu Incremental Approximate Dynamic Programming for Nonlinear Adaptive Tracking Control with Partial Observability *Journal of Guidance, Control, and Dynamics*, vol. 41, no. 12, pp. 2554–2567, 2018, doi: 10.2514/1.G003472.
- [19] Y. Zhou, E. van Kampen and Q.P. Chu An Incremental Approximate Dynamic Programming Flight Controller Based on Output Feedback *AIAA Guidance, Navigation, and Control Conference*, San Diego, California, USA, January, 2016, doi: 10.2514/6.2016-0360.
- [20] B. Sun and E. van Kampen Incremental Model-Based Heuristic Dynamic Programming with Output Feedback Applied to Aerospace System Identification and Control *2020 IEEE Conference on Control Technology and Applications*, Montreal, QC, Canada, 2020, pp. 366–371, August, 2020, doi: 10.1109/CCTA41146.2020.9206261.
- [21] B. Sun and E. van Kampen Intelligent Adaptive Optimal Control Using Incremental Model-Based Global Dual Heuristic Programming Subject to Partial Observability *Applied Soft Computing*, vol. 103, pp. 1–15, 2021, doi: 10.1016/j.asoc.2021.107153.
- [22] B. Sun and E. van Kampen Reinforcement-Learning-Based Adaptive Optimal Flight Control with Output Feedback and Input Constraints *Journal of Guidance, Control, and Dynamics*, vol. 44, no. 9, pp. 1685–1691, 2021, doi: 10.2514/1.G005715.
- [23] B. Sun and E. van Kampen Event-Triggered Constrained Control Using Explainable Global Dual Heuristic Programming for Nonlinear Discrete-Time Systems *Neurocomputing*, vol. 468, pp. 452–463, 2022, doi: 10.1016/j.neucom.2021.10.046.
- [24] Y. Zhou, E. van Kampen and Q.P. Chu Incremental Model Based Heuristic Dynamic Programming for Nonlinear Adaptive Flight Control In *Proceedings of the International Micro Air Vehicles Conference and Competition*, Beijing, China, October, 2016, url: <https://www.imavs.org/papers/2016/25.pdf>.
- [25] Y. Zhou, E. van Kampen and Q. P. Chu Incremental Model based Online Heuristic Dynamic Programming for Nonlinear Adaptive Tracking Control with Partial Observability *Aerospace Science and Technology*, vol. 105, pp. 1–14, 2020, doi: 10.1016/j.ast.2020.106013.
- [26] S. Heyer, D. Kroezen and E. van Kampen Online Adaptive Incremental Reinforcement Learning Flight Control for a CS-25 Class Aircraft *AIAA Scitech 2020 Forum*, Orlando, FL, USA, October, 2020, doi: 10.2514/6.2020-1844.
- [27] L.G. Sun, C.C. de Visser, Q.P. Chu and W. Falkena Hybrid Sensor-Based Backstepping Control Approach with Its Application to Fault-Tolerant Flight Control *Journal of Guidance, Control, and Dynamics*, vol. 31, no. 1, pp. 59–71, 2014, doi: 10.2514/1.61890.
- [28] Y. Zhou, E. van Kampen and Q.P. Chu Launch Vehicle Adaptive Flight Control with Incremental Model Based Heuristic Dynamic Programming *International Astronautical Congress*, Adelaide, Australia, September, 2017.
- [29] S. Mysore, B. Mabsout, R. Mancuso and K. Saenko Regularizing Action Policies for Smooth Control with Reinforcement Learning *IEEE International Conference on Robotics and Automation*, Xi’an, China, October, 2021, doi: 10.1109/ICRA48506.2021.9561138.
- [30] A.N. Kalliny, A.A. El-Badawy and S.M. Elkhamsy Command-Filtered Integral Backstepping Control of Longitudinal Flapping-Wing Flight *Journal of Guidance, Control, and Dynamics*, vol. 41, no. 7, pp. 1556–1568, 2018, doi: 10.2514/1.G003267.
- [31] J.A. Farrell, M. Polycarpou, M. Sharma and W. Dong Command Filtered Backstepping *IEEE Transactions on Automatic Control*, vol. 54, no. 6, pp. 1391–1395, 2009, doi: 10.1109/TAC.2009.2015562.
- [32] R.A. Hull, D. Schumacher and Z.H. Qu Design and Evaluation of Robust Nonlinear Missile Autopilots from a Performance Perspective In *Proceedings of 1995 American Control Conference*, Seattle, WA, USA, June, 1995, doi: 10.1109/ACC.1995.529235.
- [33] P. J. Werbos Advanced Forecasting Methods for Global Crisis Warning and Models of Intelligence *General Systems*, vol. 22, pp. 25–38, 1977, url: <https://gwern.net/doc/reinforcement-learning/1977-werbos.pdf>.
- [34] K. Shibata Dynamic Reinforcement Learning for Actors *arXiv preprint*, 2025, doi: 10.48550/arXiv.2502.10200.

APPENDIX

A. Derivation of incremental model

Taking the Taylor expansion of systems 6:

$$\begin{aligned}
 \alpha_{t+1} &= \alpha_t + F_{t-1}^1(\alpha_t - \alpha_{t-1}) + G_{t-1}^1(q_t - q_{t-1}) \\
 &\quad + O[(\alpha_t - \alpha_{t-1})^2, (q_t - q_{t-1})^2] \\
 q_{t+1} &= q_t + F_{t-1}^2(q_t - q_{t-1}) + G_{t-1}^2(\delta_t - \delta_{t-1}) \\
 &\quad + O[(q_t - q_{t-1})^2, (\delta_t - \delta_{t-1})^2]
 \end{aligned} \tag{35}$$

where

$$\begin{aligned}
F_{t-1}^1 &= \frac{\partial h_1[\alpha_t, \delta_t, q_t]}{\partial \alpha_t} \Big|_{\alpha_{t-1}, \delta_{t-1}, q_{t-1}} \\
G_{t-1}^1 &= \frac{\partial h_1[\alpha_t, \delta_t, q_t]}{\partial q_t} \Big|_{\alpha_{t-1}, \delta_{t-1}, q_{t-1}} \\
F_{t-1}^2 &= \frac{\partial h_2[\alpha_t, \delta_t, q_t]}{\partial q_t} \Big|_{\alpha_{t-1}, \delta_{t-1}, q_{t-1}} \\
G_{t-1}^2 &= \frac{\partial h_2[\alpha_t, \delta_t, q_t]}{\partial q_t} \Big|_{\alpha_{t-1}, \delta_{t-1}, q_{t-1}}
\end{aligned} \tag{36}$$

and $O(\cdot)$ represents higher-order terms that can be ignored if the time step t is sufficiently small.

Define state increments and control increment as

$$\begin{aligned}
\Delta \alpha_t &= \alpha_t - \alpha_{t-1} \\
\Delta q_t &= q_t - q_{t-1} \\
\Delta \delta_t &= \delta_t - \delta_{t-1}
\end{aligned} \tag{37}$$

Therefore, the incremental model can be formulated as

$$\begin{aligned}
\Delta \alpha_{t+1} &= F_{t-1}^1 \Delta \alpha_t + G_{t-1}^1 \Delta q_t \\
\Delta q_{t+1} &= F_{t-1}^2 \Delta q_t + G_{t-1}^2 \Delta \delta_t
\end{aligned} \tag{38}$$

B. Higher-level agent's critic and actor update

1) *Critic*: The gradient of $L_t^{C_1}$ with respect to ψ_1 is

$$\begin{aligned}
\frac{\partial L_t^{C_1}}{\partial \psi_{1(t)}} &= \frac{\partial L_t^{C_1}}{\partial \delta_{1(t)}} \frac{\partial \delta_{1(t)}}{\partial \psi_{1(t)}} \\
&= -\delta_{1(t)} \frac{\partial \hat{V}_1(\alpha_t, e_{\alpha(t)})}{\partial \psi_{1(t)}}
\end{aligned} \tag{39}$$

The parameter set ψ_1 is updated as

$$\psi_{1(t+1)} = \psi_{1(t)} - \eta_{C_1} \frac{\partial L_t^{C_1}}{\partial \psi_{1(t)}} \tag{40}$$

where η_{C_1} is the learning rate.

2) *Target Critic*: The target critic network is used to stabilize learning by delaying the updates:

$$\psi'_{1(t+1)} = \tau \psi_{1(t+1)} + (1 - \tau) \psi'_{1(t)} \tag{41}$$

where τ is delay factor τ , ψ'_1 is the parameter set of target critic.

3) *Actor*: The gradient of $L_t^{A_1}$ with respect to ϑ_1 is

$$\begin{aligned}
\frac{\partial L_t^{A_1}}{\partial \vartheta_{1(t)}} &= \frac{\partial [c_1(\hat{e}_{\alpha(t+1)}, q_t) + \gamma \hat{V}_1(\hat{\alpha}_{t+1}, \hat{e}_{\alpha(t+1)})]}{\partial \vartheta_{1(t)}} \\
&= \left[\frac{\partial c_1(\hat{e}_{\alpha(t+1)}, q_t)}{\partial \hat{\alpha}_{t+1}} + \gamma \frac{\hat{V}_1(\hat{\alpha}_{t+1}, \hat{e}_{\alpha(t+1)})}{\partial \hat{\alpha}_{t+1}} \right] \\
&\quad \frac{\partial \hat{\alpha}_{t+1}}{\partial q_{\text{ref}}(t)} \frac{\partial q_{\text{ref}}(t)}{\partial \vartheta_{1(t)}} \\
&= \left[\frac{\partial c_1(\hat{e}_{\alpha(t+1)}, q_t)}{\partial \hat{\alpha}_{t+1}} + \gamma \frac{\hat{V}_1(\hat{\alpha}_{t+1}, \hat{e}_{\alpha(t+1)})}{\partial \hat{\alpha}_{t+1}} \right] \\
&\quad \hat{G}_{t-1}^1 \frac{\partial q_{\text{ref}}(t)}{\partial \vartheta_{1(t)}}
\end{aligned} \tag{42}$$

The parameter set ϑ_1 is updated as

$$\vartheta_{1(t+1)} = \vartheta_{1(t)} - \eta_{A_1} \frac{\partial L_t^{A_1}}{\partial \vartheta_{1(t)}} \tag{43}$$

where η_{A_1} is the learning rate.

From an algorithmic perspective, the update of ψ_t to ψ_{t+1} can be performed multiple times until the critic loss L_{critic} falls below a specified threshold. Subsequently, the update of ϑ_t to ϑ_{t+1} can also be repeated until the actor loss L_{actor} begins to reverse direction, indicating that ϑ_t is near a local optimum. These steps constitute one iteration of approximate value iteration. The approximate value iteration can be executed for multiple times at time step t .

C. Lower-level agent's critic and actor update

1) *Critic*: The gradient of $L_t^{C_2}$ with respect to ψ_2 is

$$\begin{aligned}
\frac{\partial L_t^{C_2}}{\partial \psi_{2(t)}} &= \frac{\partial L_t^{C_2}}{\partial \delta_{2(t)}} \frac{\partial \delta_{2(t)}}{\partial \psi_{2(t)}} \\
&= -\delta_{2(t)} \frac{\partial \hat{V}(q_t, e_{q(t)})}{\partial \psi_{2(t)}}
\end{aligned} \tag{44}$$

The parameter set ψ_2 is updated as

$$\psi_{2(t+1)} = \psi_{2(t)} - \eta_{C_2} \frac{\partial L_t^{C_2}}{\partial \psi_{2(t)}} \tag{45}$$

where η_{C_2} is the learning rate.

2) *Target Critic*: Target critic is used to stabilize the learning by slowing down the network update.

$$\psi'_{2(t+1)} = \tau \psi_{2(t+1)} + (1 - \tau) \psi'_{2(t)} \tag{46}$$

where τ is delay factor, ψ'_2 is parameter set of target critic.

3) *Actor*: The gradient of $L_t^{A_2}$ with respect to ϑ_2 is

$$\begin{aligned}
\frac{\partial L_t^{A_2}}{\partial \vartheta_{2(t)}} &= \frac{\partial [c_2(\hat{e}_{q(t+1)}, \delta_t) + \gamma \hat{V}_{2\text{target}}(\hat{q}_{t+1}, \hat{e}_{q(t+1)})]}{\partial \vartheta_{2(t)}} \\
&= \left[\frac{\partial c_2(\hat{e}_{q(t+1)}, \delta_t)}{\partial \hat{q}_{t+1}} + \gamma \frac{\hat{V}_{2\text{target}}(\hat{q}_{t+1}, \hat{e}_{q(t+1)})}{\partial \hat{q}_{t+1}} \right] \\
&\quad \frac{\partial \hat{q}_{t+1}}{\partial \delta_{e(t)}} \frac{\partial \delta_{e(t)}}{\partial \vartheta_{2(t)}} \\
&= \left[\frac{\partial c_2(\hat{e}_{q(t+1)}, \delta_t)}{\partial \hat{q}_{t+1}} + \gamma \frac{\hat{V}_{2\text{target}}(\hat{q}_{t+1}, \hat{e}_{q(t+1)})}{\partial \hat{q}_{t+1}} \right] \\
&\quad \hat{G}_{t-1}^2 \frac{\partial \delta_{e(t)}}{\partial \vartheta_{2(t)}}
\end{aligned} \tag{47}$$

The parameter set ϑ_2 is updated as

$$\vartheta_{2(t+1)} = \vartheta_{2(t)} - \eta_{A_2} \frac{\partial L_t^{A_2}}{\partial \vartheta_{2(t)}} \tag{48}$$

where η_{A_2} is the learning rate.